Exploration and application of nanomedicine in atherosclerotic disease

Lobatto, M.E.

Publication date
2016
Document Version
Final published version

Chapter 6

Imaging the efficacy of anti-inflammatory liposomes in a rabbit model of atherosclerosis by non-invasive imaging

Methods in Enzymology 2012;598:211-28

Mark E. Lobatto, Claudia Calcagno, Josbert M. Metselaar, Gert Storm, Erik S. G. Stroes, Zahi A. Fayad and Willem J. M. Mulder

Abstract

Nanomedicine can provide a potent alternative to current therapeutic strategies for atherosclerosis. For example, the encapsulation of anti-inflammatory drugs into liposomes improves their pharmacokinetics and biodistribution, thereby enhancing bioavailability to atherosclerotic plaques and improving therapeutic efficacy. The evaluation of this type of experimental therapeutics can greatly benefit from *in vivo* evaluation to assess biological changes, which can be performed by non-invasive imaging techniques, such as ^{18}F-fluorodeoxyglucose positron emission tomography/computed tomography (FDG-PET/CT) and dynamic contrast enhanced magnetic resonance imaging (DCE-MRI). Here we will illustrate the methods for inducing atherosclerosis in a rabbit model, the production of anti-inflammatory liposomes and monitoring of therapeutic efficacy of experimental therapeutics with the above-mentioned imaging techniques.

Introduction

The primary cause of cardiovascular disease, atherosclerosis, is a chronic systemic disease characterized by subendothelial lipid deposits with an inflammatory reaction[1]. To date, most interventions for the treatment of atherosclerosis have focused on altering systemic lipid levels. A promising alternative approach to reduce the risk of vascular events caused by atherosclerosis is to directly target local inflammation at the level of the vessel wall[2]. A potential drawback of an anti-inflammatory strategy is the thin line between inhibiting local inflammation in the vessel wall versus inducing systemic immuno-suppression. One way to limit the systemic effects of an anti-inflammatory regimen is to attain local delivery of drugs by encapsulating anti-inflammatory drugs in nanoparticles, for example in liposomes. This method has been investigated in a variety of diseases implicated with inflammation, including cancer, multiple sclerosis, and rheumatoid arthritis[3]. Drugs encapsulated in long-circulating liposomes accumulate at inflammatory regions to a higher extent than the free drug due to enhanced vascular permeability[4]. At these sites, long-circulating nanoparticles will extravasate from the circulation and stay retained locally. This targeting phenomenon is commonly referred to as the enhanced permeability and retention (EPR) effect[5].

Previously, it has been established that polyethylene glycol (PEG)-coated liposomes, encapsulating the anti-inflammatory drug prednisolone phosphate, effectively target atherosclerotic lesions in a rabbit model of atherosclerosis, and aggressively attenuate atherosclerotic plaque inflammation[6]. To a large degree this is attributed to nonspecific targeting of plaques, which results in an improved bioavailability of the liposomal formulation over free circulating corticosteroids.

Since atherosclerosis is a systemic disease of the vasculature, the evaluation of therapeutic interventions was traditionally based on the incidence of cardiovascular events or on secondary endpoints, such as measuring systemic lipid levels or circulating biomarkers. The past two decades have witnessed tremendous progress in the direct visualization of atherosclerotic plaque morphology and activity by non-invasive imaging[7]. These imaging techniques include various forms of magnetic resonance imaging (MRI) as well as positron emission tomography. One of the most exciting developments in non-invasive imaging of atherosclerosis is the possibility to evaluate therapeutic efficacy at earlier stages of drug development, without the need, for example, to monitor major cardiac events in longitudinal studies[8]. This strategy can vastly speed up the process of drug development or rejection, and facilitates the translation of therapeutics into clinical medicine. A variety of imaging techniques for the evaluation of therapeutic efficacy are now in clinical use, such as intravascular ultrasound of coronary arteries, or the measurement of carotid intima-media thickness by ultrasound[9,10]. Other modalities, which provide information on biological plaque processes instead of plaque morphology, such as FDG-PET/CT, have also been included in clinical trials recently[11].

FDG-PET/CT is used to visualize, quantify and characterize atherosclerotic plaque inflammation non-invasively by detecting early metabolic changes in response to treatment, before changes in plaque size and morphology are appreciable[12]. Additional information on plaque volume, composition, endothelial permeability and plaque neovascularization can be provided by high-resolution MRI and DCE-MRI[7,13].

In larger animal models of atherosclerosis, such as the rabbit, the aforementioned clinical imaging methods can be applied to evaluate therapeutic efficacy. In this chapter, we will describe the preparation and development of an experimental rabbit model of atherosclerosis, as well as methods for producing clinically translatable liposomal anti-inflammatory formulations, and we will conclude with providing a guideline on the setup and evaluation of therapeutic efficacy of such liposomal nanoparticles with the non-invasive imaging modalities, FDG-PET/CT and DCE-MRI.

Experimental animal model of atherosclerosis

A variety of animal models of atherosclerosis are available, ranging from genetically engineered mouse models to Watanabe hyperlipedimic rabbits and Yukutan swine models. For the purpose of the studies described here, we recommend New Zealand White rabbits. These rabbits have several advantages over other animal models, as they are large enough to be imaged on clinical scanners with sufficient spatial resolution, are easy to handle, and the aorta is less prone to be

affected by motion artifacts, all preferable for the imaging procedures described later on.

Procedure: Balloon angioplasty of the aorta in a rabbit model

Although there is some degree of variability in the procedures used to induce atherosclerosis in this animal model, most methods include a combination of a high cholesterol diet for varying periods of time and a balloon injury of the aorta. The balloon injury will denude the aorta of endothelial cells and will enhance the uptake of cholesterol and macrophages in the vessel wall, thereby creating atherosclerotic lesions[14].

Rabbits can be purchased from several vendors and are usually four months old at the initiation of the atherogenic diet[15]. We use a combination of a high cholesterol diet (4.7% palm oil and 0.3% cholesterol-enriched diet, and 4.85% palm oil and 0.15% cholesterol-enriched diet; Research Diet Inc., New Jersey, USA) and a repeated balloon injury of the aorta by a femoral angioplasty under fluoroscopic guidance two and six weeks after diet initiation. Procedures are performed under sterile conditions and under general anesthesia while monitoring vital functions. Anesthesia is induced by an intramuscular injection of Ketamine (20 mg/kg;Vedco, Missouri, USA) and Xylazine (10 mg/kg; Vedco, Missouri, USA). After general anesthesia, the inguinal area of the extremity that will undergo angioplasty is shaved and prepped with povidone-iodine solution. The rabbit is then placed in the supine position with the hindlimb stretched out, and the foot is taped down to the operating table to ensure a stable position of the extremity, and subsequently covered in sterile drapes in appropriate fashion. An approximately 5–7 cm longitudinal skin incision is made in the medial thigh, starting at the center of the inguinal ligament with care to avoid damaging the underlying structures. After dissection, the femoral neurovascular bundle can be identified in the proximal inguinal region. When dissecting the femoral artery from the surrounding tissue, special care should be taken to avoid damage to the femoral nerve. Care must also be taken to circumferentially dissect the vessel; once a stretch of 2–3 cm has been freed from the surrounding tissue, the blood flow is constricted by applying a suture to the distal end of the exposed femoral artery, using a silk 2-0 suture (Ethicon) to ease catheter insertion later on. In addition, 1.0% Lidocaine can be added for the purpose of attaining vasodilatation. To avoid blood loss and to maintain overview, a vascular loop can be placed around the proximal part of the artery. An incision is made in the artery length-wise with a #11 scalpel blade, and a catheter introducer (BD, New Jersey, USA) is inserted to ease the introduction of a 4-F Fogarty embolectomy catheter (Edwards Lifesciences, California, USA) (Figure 1A). Once the catheter is inserted, the vascular loop is removed to advance the catheter up to the thoracic descending aorta. The catheter and attached manometer can be filled with Iopamidol (Bracco Diagnostics, New Jersey, USA) to adequately track the balloon under fluoroscopic guidance.

The balloon is inflated gently to a pressure of 2.0 atm with a manometer. To denude the aorta of endothelial cells the catheter is pulled back over the entire length of the aorta down to the iliac bifurcation (Figure 1B). While retracting the catheter, the balloon should be deflated slowly when encountering resistance to avoid creating aortic aneurysms. The pullback procedure is repeated two additional times. The catheter is removed subsequently, and the femoral artery is ligated. The procedure is completed when hemostasis is ensured, the subcutaneous tissue is approximated with 2 interrupted Vicryl 3-0 sutures, and the skin is closed with a Prolene continuous monofilament suture 2.0 (Ethicon). The same procedure is repeated four weeks later from the contralateral extremity. After six months of initiating the diet, the rabbits will have grown advanced atherosclerotic lesions, as shown in Figure 1C.

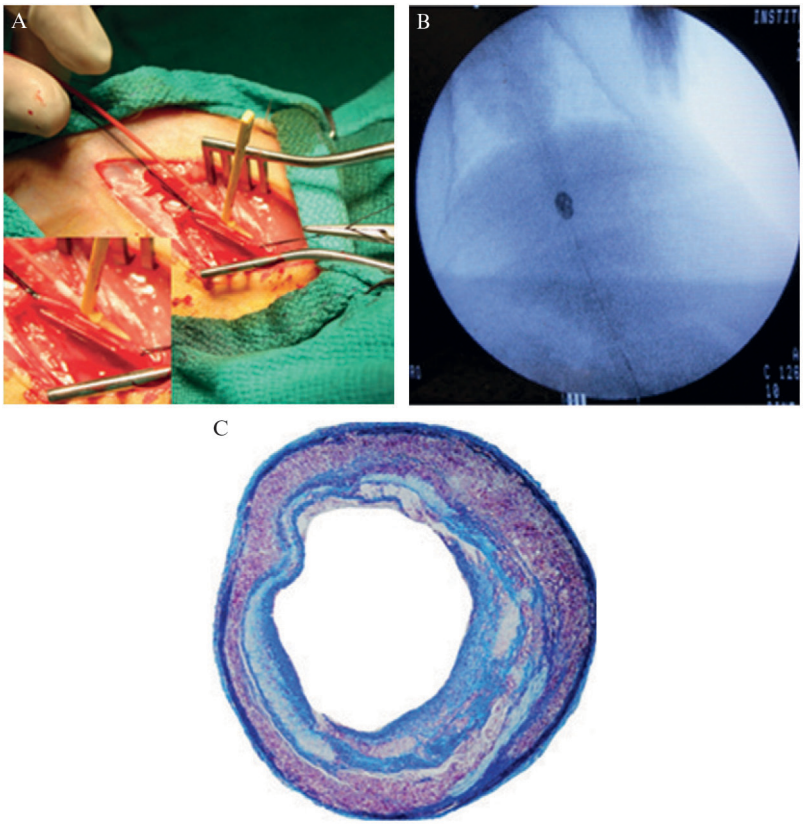

Figure 1. The induction of atherosclerosis in a New Zealand White rabbit. (A) After 2 and 6 weeks of a high cholesterol-enriched diet, a femoral angioplasty is performed by exposing the femoral artery under surgical conditions and introducing a 4-F embolectomy catheter. (B) The balloon is subsequently inflated, while pulling back the inflated balloon over the length of the aorta to denude the aorta of endothelial cells. (C) After 6 months rabbits will have advanced atherosclerotic lesions, evidenced by histology with a Masson's trichrome stain.

Liposome preparation

Liposome preparation in the laboratory

Long-circulating PEG liposomes can be prepared of a mixture of dipalmitoyl phosphatidyl choline (DPPC), cholesterol, and PEG 2000 distearoyl phosphatidylethanolamine (PEG-DSPE) in a molar ratio of 62%, 33% and 5%, respectively. Anti-inflammatory properties are acquired by encapsulating a corticosteroid in the aqueous interior of the liposome. To ensure an optimal inclusion efficiency, the water-soluble disodium phosphate ester derivative of the corticosteroid is used. Upon release at the target site, mainly induced by local phagocytes and extracellular enzymes, the inactive phosphate derivative is converted into the active drug. To obtain the desired long-circulating behavior, the liposomes need to comply with a particle diameter specification roughly between 75 and 150 nm. However, to avoid problems with sterile filtration on the one hand and with low steroid content on the other hand, the liposomes are kept below 120 nm and above 80 nm, respectively. The incorporation efficiency of the drug in liposomes is typically between 1.5-3% at a molar lipid starting concentration of 100 mM and is dependent on particle size. This translates to a final content between 1.5 and 3.0 mg/ml of corticosteroid within the formulation.

The most straightforward manufacturing method of lab scale liposomal corticosteroid batches involves extrusion. Briefly, a lipid solution is prepared in ethanol, containing DPPC, cholesterol

and PEG-DSPE in a round bottom flask, which is then evaporated under rotation to create a lipid film. This lipid film is hydrated with an aqueous solution of corticosteroid phosphate. The resulting coarse lipid dispersion is subsequently downsized by repeated extrusion at elevated temperatures (above 60 °C) through a series of polycarbonate filter membranes. Unencapsulated prednisolone is removed by dialysis against 0.9% phosphate buffered saline using dialysis cassettes with a molecular weight cut-off value of 30,000 kD. Extrusion is a suitable method for lab batches of corticosteroid liposomes up to 100 ml.

Good manufacturing practice (GMP) production of anti-inflammatory liposomes

Manufacturing of larger quantities by extrusion is more complex because it requires large and expensive equipment in which temperature is difficult to control. Stepping up from small to large scale extrusion equipment does not necessarily lead to a product with comparable specifications. Furthermore, the formulation shows the tendency to clog the extrusion membrane and changing the extrusion membranes in large-scale equipment during the manufacturing process is not straightforward. Therefore, to manufacture larger batches of liposomal corticosteroid product under GMP conditions, we opted for an alternative method named high-shear homogenization. In this method the coarse lipid dispersion is led through an interaction chamber under high pressure, which creates high flow speeds and shear forces that effectively downsize the liposomes. Homogenization allows a more continuous process that leads to identical results, whether small or large volumes of formulations are processed, as long as the manufacturing circumstances (temperature and pressure) are kept the same.

To manufacture 1 l of corticosteroid liposomes under GMP conditions, 62.5 g corticosteroid phosphate derivative is dissolved in 450 ml of sterile water for injection. The lipid components (45.0 g DPPC, 13.4 g PEG-DSPE, and 12.6 g cholesterol) are dissolved in 50 ml ethanol by heating to 70 °C under continuous stirring. The alcoholic lipid solution is then injected into the aqueous prednisolone sodium phosphate solution under vigorous stirring, creating a coarse lipid dispersion.

Downsizing the liposomes to the desired particle diameter occurs by high-shear homogenization. The homogenizer is first sterilized by continuous circulation of 500 ml 1 M sodium hydroxide and subsequently rinsed with phosphate buffered water for injections until the pH reaches 7.4. The coarse lipid dispersion is homogenized by three consecutive runs, while keeping the temperature of the dispersion between runs at 70 °C, by placing the lipid dispersion on a hot magnetic stirrer. After the third run the fine liposome dispersion is gradually cooled down to room temperature.

To clear the formulation from unencapsulated corticosteroid and ethanol, the fine liposome dispersion is transferred to a sterile crossflow filtration unit, and filtered using polysulfonate membrane capsules with a cut off of 100 kD. A sterile phosphate buffered (pH 7.6) sucrose solution (10%) is prepared and added to the retentate in the filtration unit to compensate for the loss of permeate from the unit (which is unencapsulated aqueous corticosteroid solution). When a total of 15 l sucrose solution has been added, the dispersion can be considered devoid of unencapsulated prednisolone sodium phosphate and ethanol.

Finally, the liposome dispersion is sterile-filtered by dead-end filtration using a 0.45 - 0.2 μm Sartobran-P filter unit connected to a membrane pump. The filtered dispersion is collected into 10 ml injection vials using 1.6 mm x 1.6 mm platinum-catalyzed silicone tubing. The injection vials are subsequently stoppered, sealed with aluminum caps and labeled. The final liposomal product is stored between 2 and 8 °C. The most important quality control tests and specificati¬ons with regard to the final liposomal corticosteroid product are listed in Table 1.

Shelf life stability studies with the liposomal corticosteroid product have indicated that it remains stable for at least 2 years when stored between 2 and 8 °C. During this time no significant changes in particle size was observed, nor do measurable amounts of the incorporated corticosteroid leak from the liposomal interior. The chemical stability of both the active ingredient and the lipid excipients remains excellent under these storage conditions. Storage at ambient or higher temperatures indicates that cholesterol will eventually pose the most critical stability problem, as it slowly degrades at these temperatures.

Item/test method	Specification
1. Appearance	A clear to mildly turbid fluid
2. Dynamic light scattering	
Particle diameter	80–120 nm
Polydispersity index	$\leq$ 0.25
3. HPLC assay encapsulated drug identification	Retention time of the corticosteroid reference standard equals the retention time of the liposomal corticosteroid
Content	1.5–3.0 mg/ml
Content uniformity	All vials within 85.0–115.0%, relative standard deviation less or equal to 6.0%
4. HPLC assay free drug in permeate	$\leq$ 0.05 mg/ml
5. HPLC assay lipid excipients identification	Retention time of the lipid reference standard equals the retention time of the lipid in the product
Content	80–120% of the starting lipid concentration in the formulation
6. pH of the dispersion	Within the range of 6.50–8.50
7. Bacterial endotoxins	$<$20 EU/vial
8. Sterility	Sterile (as determined by a Steritest Compact test (Millipore, Massachusetts, USA))
9. Residual ethanol	$<$100 ppm

Table 1. Quality control tests and specifications of anti-inflammatory liposomes

Imaging as a readout for therapeutic efficacy of drugs in atherosclerosis

^{18}F-FDG in combination with PET/CT is used as a molecular imaging technique to assess metabolically active processes and is the gold standard for detection of metastases in cancer. Recently, several studies have demonstrated that ^{18}F-FDG uptake correlates with atherosclerotic plaque inflammation. Human carotid arteries that are implicated in stroke have shown an increased uptake of ^{18}F-FDG. In addition, increased uptake has also been observed in patients with acute coronary syndromes[16]. FDG-PET/CT is therefore increasingly used as a marker to assess metabolically active atherosclerotic plaques, as well as to assess the therapeutic efficacy of anti-atherosclerosis drugs[12]. This technique can be executed with high reproducibility, which is of major importance for drug efficacy studies[17]. For the purpose of this chapter we will describe a technique to measure drug efficacy of experimental therapeutics in a rabbit model.

FDG-PET/CT image acquisition

FDG-PET/CT imaging of rabbits can be performed using clinically available PET/CT scanners. Rabbits have to be fasted for 4 h prior to radiotracer injection to avoid interference with ^{18}F-FDG uptake, while water can be provided *ad libitum*. With a catheter placed in the marginal ear vein, rabbits are injected with 1 mCi/Kg ^{18}F-FDG, followed by a 5 ml saline flush. It is useful to note the exact amount of ^{18}F-FDG that has been injected, as well as the weight of the animal, as this is essential for subsequent image analysis. For the interpretation of the data it is also recommended to have ^{18}F-FDG circulate for 180 min prior to imaging, as it has been reported that this will maximize the contrast between the plaque and background activity, and will therefore give a more accurate representation of actual ^{18}F-FDG plaque uptake[18]. For the evaluation of therapeutic efficacy it is required to obtain a scan prior to injection of the drug to be evaluated. Time points after therapeutic drug administration can be chosen according to

drug half-life and expected duration of drug activity. Rabbits are imaged supine under general anesthesia, dosed as earlier, while secured with a blanket. It is vital to empty the bladder with a catheter before imaging as the renal clearance of FDG and ensuing accumulation in the bladder will heavily impair the analysis of FDG uptake in the distal aorta.
Rabbits are scanned in a single-bed position in 3-dimensional (3D) mode for 10 min, covering the region of the thoracic descending aorta down to the iliac bifurcation (approximately 15.5 cm). Reconstruction is then performed which typically can give a reconstructed slice thickness of 4.25 mm.

FDG-PET/CT image analysis

For image analysis, the PET/CT images are then calibrated to the injected dose of ^{18}F-FDG and animal weight. The images can be analyzed on the locally available workstation by measuring arterial ^{18}F-FDG uptake in the aorta, after drawing a region of interest (ROI) around the aorta on slices of co-registered transaxial PET/CT images. A suggestion is to start at the superior mesenteric artery and end at the iliac bifurcation to ensure that the same anatomic region is covered in each individual rabbit. On each image slice, the mean standard uptake value (SUV) of ^{18}F-FDG in the artery is calculated as the mean pixel activity within the ROI. The SUV is the decay-corrected tissue concentration of ^{18}F-FDG (in kBq/g), corrected for the injected ^{18}F-FDG dose and body weight (in kBq/g); this is a well-recognized method for the analysis of PET data. To ensure proper data for SUV comparison with serially scanned animals it is advised to use the exact same injection and imaging acquisition times. After analysis of the aorta, the SUV average can be compared to pre-injection data. Although the value of FDG-PET data is becoming increasingly validated, it is suggested to confirm and correlate values with immunohistochemistry. Macrophage density count has been used as the histological standard to validate SUV, which can be obtained through immunohistochemical staining with RAM-11 (Dako, California, USA)[19]. Because nuclear imaging is involved with this technique, it is essential to involve the radiation safety officer within the local institute to account for relevant safety precautions.

DCE-MRI background

DCE-MRI is a non-invasive imaging technique used to study the extent and characteristics of the microvasculature in many physiological and pathological instances[20–22]. It consists of the rapid serial acquisition of MRI images during the injection of a contrast agent (CA; most often a gadolinium chelate). The CA acts by shortening the proton relaxation times of target tissues, which results in a change in the MR signal during data acquisition. After appropriate conversion to concentration, CA uptake curves are analyzed using either compartmental modeling or non-model based approaches to infer the extent and properties of tissue microvasculature[23–25].
In recent years DCE-MRI has been adopted to study the formation of new vessels, neovascularization, in atherosclerotic plaques in both rabbit models as well as human subjects with carotid disease[26–28]. The extent of neovascularization in atherosclerotic disease has been shown to correlate with inflammation, and plaques that are prone to rupture[29]. Current approaches for DCE-MRI of atherosclerosis can be classified into "bright blood" and "black blood" techniques. Bright blood techniques are T1-weighted, spoiled gradient echo (SPGR)-based acquisitions, and allow the determination of the CA concentration in the blood plasma (the so called arterial input function, AIF), which is required to extract kinetic parameters. Using bright blood acquisitions, a positive significant correlation between DCE-MRI measures and neovascularization in human carotid plaques has been demonstrated[30]. A positive significant correlation between DCE-MRI measures and several atherosclerosis risk factors has been confirmed as well[30]. Because of their intrinsically poor vessel lumen/wall delineation, bright blood techniques are usually not suited for imaging early atherosclerotic lesions and/or animal models, where the vessel wall thickness can be less than 2 mm. In these cases, black blood techniques are advantageous.
Black blood techniques typically consist of T1-weighted turbo spin echo (TSE) acquisitions, and allow better vessel lumen/wall delineation than bright blood techniques. Since they do not allow for direct acquisition of the AIF from the dynamic scan, either a population AIF, relative modeling or non-model based approaches are used for their analysis. Using non-model based approaches, a positive significant relationship between neovascularization in aortic plaque of atherosclerotic rabbits and the DCE-MRI parameter area under the curve (AUC) is observed[26].

Additionally, good reproducibility of the technique and its potential as read-out for anti-inflammatory therapy was shown recently[31].

DCE-MRI acquisition

The acquisition of DCE-MRI scans is performed under anesthesia (dosed as earlier). If necessary, another half a dose of anesthesia can be administered 45-60 min after induction during long scanning procedures, or anesthesia can be sustained by the use of Isofluorane. Slightly different protocols can be used for DCE-MRI acquisition. Here we will describe a comprehensive image acquisition and analysis protocol.

Doses of contrast agent (CA) are 0.1 or 0.2 mmol/kg for the full dose DCE scan (depending on the desired signal-to-noise ratio, SNR) and 0.01 mmol/kg for the test bolus. The contrast agent can be administered by either manual injection or using a power injector. If the manual injection is chosen, one syringe is prepared with the full dose of CA, one syringe with the test bolus dose diluted to the volume of the full dose, and 2 syringes with 10 ml saline. When performing manual injections one researcher needs to be inside the MRI room during the dynamic scan. For both test and full dose administration, after acquisition of a few pre-contrast frames, the CA is first injected through intravenous injection, followed by the saline flush. If the CA is delivered through a power injector, syringes are prepared with a test dose, a full dose and saline. If the power injector cannot deliver fractions of ml, both CA doses will be diluted to the same lowest possible volume. After placing the syringes on the power injector, the line is filled with saline and checked for the presence of air. After positioning the rabbit in the MRI (see below), the line is connected to the catheter. The injection can be delivered at a rate of 0.5 ml/s, after a chosen number (minimum of 3) of pre-contrast images. The set of syringes will have to be exchanged between the test and full dose injection.

The rabbits are scanned with a conventional volume knee coil on the clinically available MRI scanner, with sufficient padding to support the head and legs of the animal during imaging. The animal is positioned in the coil, head-first supine, making sure that the abdomen is approximately at the center of the coil. If a power injector is used, the line is connected to the catheter in the marginal ear vein.

After performing localizer scans, a time-of-flight acquisition should be performed from the renal artery to the iliac bifurcation. This acquisition is useful for slice planning of subsequent scans and for serial studies to identify anatomical fiducial markers to be used for image co-registration. Subsequently, conventional black blood TSE acquisitions for morphological plaque characterization are performed. Black blood imaging can be achieved using spatial saturation or double inversion pulses. Depending on the scope of the study, T1 and/or T2 and/or proton density (PD) weighted imaging is performed. Typical imaging parameters for T1/T2/PD weighted images are as follows: acquisition type, 2D; slice thickness, 3 mm; inter-slice gap, 0.3 mm; number of slices, 25-30; echo time (TE), 5.6/39/5.6 ms; repetition time (TR), 800/2000/2000 ms; FOV, 12 × 12 cm^2; in-plane spatial resolution, 0.5 x 0.5 mm^2; echo train length, 7; and signal averages, 16. Spectral fat suppression is applied to null the signal from the peri-adventitial fat. Following anatomical images, a test-bolus[32] is acquired to sample the AIF, using a single slice, single-shot saturation prepared gradient echo acquisition. Typical imaging parameters are: acquisition type, 2D; slice thickness, 3-mm; TE, 2.1 ms; TR, 4.3 ms; flip angle (FA), 12 degrees; FOV, 12 × 12 cm^2; in-plane spatial resolution, 1 x 1 mm^2; and signal averages, 1; time resolution ~0.5 s; acquisition duration, ~3 min.

For the purpose of signal intensity normalization, a SPGR PD weighted image without saturation preparation is acquired before the test bolus, using the same imaging parameters detailed below, except for FA (4 degrees) and TR (300 ms). Following test-bolus acquisition, a group of slices is selected for DCE-MRI based on the pre-contrast TSE scans. Before DCE acquisition, T1 mapping is acquired with a method of choice[33] to facilitate signal conversion to concentration during the analysis process. For the purpose of signal normalization, a TSE PD-weighted scan can be performed on the slices selected for DCE imaging, using the same imaging parameters detailed above (if not acquired before). T1-weighted black-blood DCE-MRI is performed on selected axial slices. Typical imaging parameters are as follows: acquisition type, 2D; slice thickness, 3 mm; inter-slice gap, 0.3 mm; number of slices, 4-6; TE, 5-10 ms; TR, 400-700 ms; FOV, 12 × 12 cm^2; in-plane spatial resolution, 0.5 x 0.5 mm^2; echo train length, 7-9; and signal averages, 1; time resolution: 20-40 s; acquisition duration 10-15 min. Following DCE, a T1

weighted post-contrast image of the same slices can be acquired with the same parameters used for DCE acquisition (except increased number of averages) for vessel wall delineation.

DCE-MRI analysis

After de-noising and intra-series co-registration for image analysis[34], ROIs are placed in the vessel lumen and wall (for test-bolus and full-dose scan respectively) and propagated through the dynamic series. After appropriate scaling MR signal values, AIF and vessel wall ROI curves can be converted to concentration by choosing one of the following equations[33]:

$$C(t) \propto \frac{(\mathrm{SI}(t) - \mathrm{SI}(0))}{\mathrm{SI}(0)}, \tag{1}$$

where *C(t)* is the CA concentration at time *t*, *SI(t)* is the MR signal at time *t*, and *SI(0)* is the pre-contrast MR signal.

$$\mathrm{SI}(t) = M_0 \frac{\sin\alpha(1 - E1(t))}{1 - E1(t)\cos\alpha}, \quad \text{where } E1(t) = \mathrm{e}^{-TR/T1(t)}, \tag{2}$$

where M_0 is the bulk magnetization, α is the FA and *T1(t)* is the longitudinal relaxation time at time *t*. After normalizing for either a PD-weighted image or the pre-contrast MR signal to account for M_0 , this equation can be solved for *T1(t)*. The CA concentration can then be calculated as:

$$\frac{1}{T1(t)} = \frac{1}{T1(0)} + \mathrm{r1} \cdot C(t), \tag{3}$$

where T1(0) is the pre-contrast T1 (which can be either calculated from a T1 mapping sequence or assumed), and r1 is the contrast agent relaxivity (which can be found in the literature).

Once converted to concentration, the test bolus has to be linearly scaled to the full-dose injected and corrected for hematocrit, before being used for kinetic modeling. It is also worth mentioning that since the values derived from Eq. (1) are only deemed linearly proportional to the real concentration and the linearity constant may vary depending on the acquisition used, this method should not be used if test bolus data are used for analysis. After conversion to concentration, parameters can be extracted from the DCE data using the following approaches:

1) if test bolus data are available, either a regular or modified Tofts model can be used[25].
2) if only black blood data are available, kinetic modeling can still be performed if a population AIF is available from the literature[35] or previous experiments. In alternative, non-model based approaches[23] or relative modeling approaches[36] can be used.

Parameters extracted from kinetic modeling can provide information about the extent of plaque neovascularization (v_p, fractional blood volume), blood flow/permeability (K^{trans}, and K_{ep}, the transfer constants from the tissue to the plasma compartments) and the distribution volume of the CA (v_e, the fractional extra-vascular extracellular space volume)[25]. These parameters can give an indication about the extent and characteristics of plaque neovasculature and inflammation, and track their changes upon intervention with anti-inflammatory therapies.

Kinetic modeling is typically performed using in-house software, using either non-linear or linear least squares methods when possible. Among non-model based parameters, despite its unclear relationship with physiological variables, the AUC of the normalized signal intensity versus time, has been correlated positively with plaque neovascularization, and was proven to be useful in tracking the response to anti-inflammatory therapy seen in Figure 2[6,13,31].

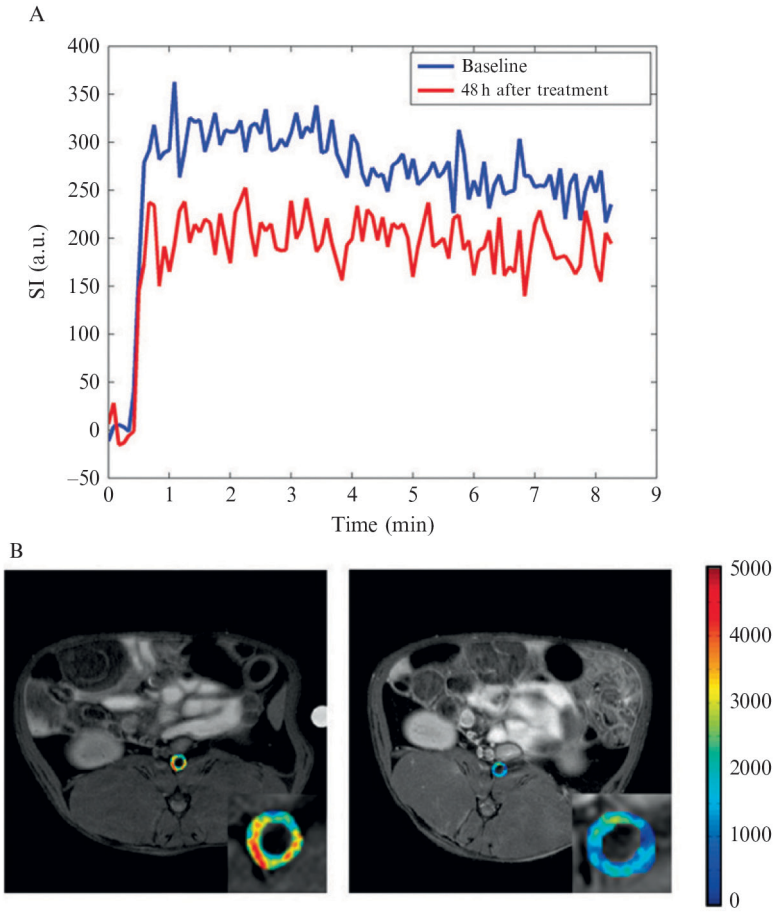

Figure 2. Evaluating therapeutic efficacy of experimental therapeutics by dynamic contrast enhanced MRI. (A) An example of a graph showing a decrease in area under the curve (AUC) in response to treatment of liposome-encapsulated prednisolone phosphate in a rabbit. (B) Overlays on anatomical MR images of AUC maps on the aorta display changes before (left) and 2 days after treatment (right). (B) reprinted with permission from Lobatto et al.[6] ©2010 American Chemical Society.

Concluding remarks

Although considerable progress has been made in the treatment of atherosclerosis, there is a continuous search and necessity for new methods to manage this disease. The use of nanoparticles encapsulating anti-inflammatory drugs targeting the atherosclerotic vessel wall can be a very efficient strategy in the right setting, for example, after a cardiovascular event, to accomplish systemic vascular silencing of inflammation to minimize future events. The methods for creating experimental atherosclerotic lesions and formulating anti-inflammatory liposomes are well-established nowadays, although the particular combination for this application is novel. Importantly, the ability of non-invasive imaging modalities, such as FDG-PET/CT and DCE-MRI, to provide early insights into drug efficacy of experimental therapeutics can greatly speed up the process of drug development, and will facilitate translating nanotherapeutics into clinical medicine.

References

1. Libby, P. Inflammation in Atherosclerosis. Nature 2002, 420, 868–874.
2. Libby, P.; Ridker, P. M.; Hansson, G. K. Progress and Challenges in Translating the Biology of Atherosclerosis. Nature 2011, 473, 317–325.
3. Metselaar, J. M.; Storm, G. Liposomes in the Treatment of Inflammatory Disorders. Expert Opin Drug Deliv 2005, 2, 465–476.
4. Maurer, N.; Fenske, D. B.; Cullis, P. R. Developments in Liposomal Drug Delivery Systems. Expert Opin Biol Ther 2001, 1, 923–947.
5. Fang, J.; Nakamura, H.; Maeda, H. The EPR Effect: Unique Features of Tumor Blood Vessels for Drug Delivery, Factors Involved, and Limitations and Augmentation of the Effect. Adv Drug Deliv Rev 2011, 63, 136–151.
6. Lobatto, M. E.; Fayad, Z. A.; Silvera, S.; Vucic, E.; Calcagno, C.; Mani, V.; Dickson, S. D.; Nicolay, K.; Banciu, M.; Schiffelers, R. M.; et al. Multimodal Clinical Imaging to Longitudinally Assess a Nanomedical Anti-Inflammatory Treatment in Experimental Atherosclerosis. Mol Pharm 2010, 7, 2020–2029.
7. Sanz, J.; Fayad, Z. A. Imaging of Atherosclerotic Cardiovascular Disease. Nature 2008, 451, 953–957.
8. Lindsay, A. C.; Choudhury, R. P. Form to Function: Current and Future Roles for Atherosclerosis Imaging in Drug Development. Nat Rev Drug Discov 2008, 7, 517–529.
9. de Groot, E.; van Leuven, S. I.; Duivenvoorden, R.; Meuwese, M. C.; Akdim, F.; Bots, M. L.; Kastelein, J. J. Measurement of Carotid Intima-Media Thickness to Assess Progression and Regression of Atherosclerosis. Nat Clin Pr. Cardiovasc Med 2008, 5, 280–288.
10. Nissen, S. E.; Tsunoda, T.; Tuzcu, E. M.; Schoenhagen, P.; Cooper, C. J.; Yasin, M.; Eaton, G. M.; Lauer, M. A.; Sheldon, W. S.; Grines, C. L.; et al. Effect of Recombinant ApoA-I Milano on Coronary Atherosclerosis in Patients with Acute Coronary Syndromes: A Randomized Controlled Trial. JAMA 2003, 290, 2292–2300.
11. Fayad, Z. A.; Mani, V.; Woodward, M.; Kallend, D.; Abt, M.; Burgess, T.; Fuster, V.; Ballantyne, C. M.; Stein, E. A.; Tardif, J.-C.; et al. Safety and Efficacy of Dalcetrapib on Atherosclerotic Disease Using Novel Non-Invasive Multimodality Imaging (dal-PLAQUE): A Randomised Clinical Trial. Lancet 2011, 378, 1547–1559.
12. Rudd, J. H.; Narula, J.; Strauss, H. W.; Virmani, R.; Machac, J.; Klimas, M.; Tahara, N.; Fuster, V.; Warburton, E. A.; Fayad, Z. A.; et al. Imaging Atherosclerotic Plaque Inflammation by Fluorodeoxyglucose with Positron Emission Tomography: Ready for Prime Time? J Am Coll Cardiol 2010, 55, 2527–2535.
13. Calcagno, C.; Mani, V.; Ramachandran, S.; Fayad, Z. A. Dynamic Contrast Enhanced (DCE) Magnetic Resonance Imaging (MRI) of Atherosclerotic Plaque Angiogenesis. Angiogenesis 2010, 13, 87–99.
14. Weidinger, F. F.; McLenachan, J. M.; Cybulsky, M. I.; Fallon, J. T.; Hollenberg, N. K.; Cooke, J. P.; Ganz, P. Hypercholesterolemia Enhances Macrophage Recruitment and Dysfunction of Regenerated Endothelium after Balloon Injury of the Rabbit Iliac Artery. Circulation 1991, 84, 755–767.
15. Fitzgerald, K. T.; Holladay, C. A.; McCarthy, C.; Power, K. A.; Pandit, A.; Gallagher, W. M. Standardization of Models and Methods Used to Assess Nanoparticles in Cardiovascular Applications. Small 2011, 7, 705–717.
16. Rogers, I. S.; Nasir, K.; Figueroa, A. L.; Cury, R. C.; Hoffmann, U.; Vermylen, D. A.; Brady, T. J.; Tawakol, A. Feasibility of FDG Imaging of the Coronary Arteries: Comparison between Acute Coronary Syndrome and Stable Angina. JACC Cardiovasc Imaging 2010, 3, 388–397.
17. Rudd, J. H.; Myers, K. S.; Bansilal, S.; Machac, J.; Rafique, A.; Farkouh, M.; Fuster, V.; Fayad, Z. A. (18) Fluorodeoxyglucose Positron Emission Tomography Imaging of Atherosclerotic Plaque Inflammation Is Highly Reproducible: Implications for Atherosclerosis Therapy Trials. J Am Coll Cardiol 2007, 50, 892–896.
18. Rudd, J. H.; Warburton, E. A.; Fryer, T. D.; Jones, H. A.; Clark, J. C.; Antoun, N.; Johnstrom, P.; Davenport, A. P.; Kirkpatrick, P. J.; Arch, B. N.; et al. Imaging Atherosclerotic Plaque Inflammation with [18F]-Fluorodeoxyglucose Positron Emission Tomography. Circulation 2002, 105, 2708–2711.
19. Zhang, Z.; Machac, J.; Helft, G.; Worthley, S. G.; Tang, C.; Zaman, A. G.; Rodriguez, O. J.; Buchsbaum, M. S.; Fuster, V.; Badimon, J. J. Non-Invasive Imaging of Atherosclerotic Plaque Macrophage in a Rabbit Model with F-18 FDG PET: A Histopathological Correlation. BMC Nucl Med 2006, 6, 3.
20. Choyke, P. L.; Dwyer, A. J.; Knopp, M. V. Functional Tumor Imaging with Dynamic Contrast-Enhanced Magnetic Resonance Imaging. J. Magn. Reson. Imaging 2003, 17, 509–520.
21. Notohamiprodjo, M.; Reiser, M. F.; Sourbron, S. P. Diffusion and Perfusion of the Kidney. Eur. J. Radiol. 2010, 76, 337–347.
22. Padhani, A. R. Dynamic Contrast-Enhanced MRI in Clinical Oncology: Current Status and Future Directions. J. Magn. Reson. Imaging 2002, 16, 407–422.
23. Roberts, C.; Issa, B.; Stone, A.; Jackson, A.; Waterton, J. C.; Parker, G. J. M. Comparative Study into the Robustness of Compartmental Modeling and Model-Free Analysis in DCE-MRI Studies. J. Magn. Reson. Imaging 2006, 23, 554–563.
24. Sourbron, S. Technical Aspects of MR Perfusion. Eur. J. Radiol. 2010, 76, 304–313.
25. Tofts, P. S.; Brix, G.; Buckley, D. L.; Evelhoch, J. L.; Henderson, E.; Knopp, M. V; Larsson, H. B.; Lee, T. Y.; Mayr, N. A.; Parker, G. J.; et al. Estimating Kinetic Parameters from Dynamic Contrast-Enhanced T(1)-Weighted MRI of a Diffusable Tracer: Standardized Quantities and Symbols. J. Magn. Reson. Imaging 1999, 10, 223–232.
26. Calcagno, C.; Cornily, J.-C.; Hyafil, F.; Rudd, J. H. F.; Briley-Saebo, K. C.; Mani, V.; Goldschlager, G.; Machac, J.; Fuster, V.; Fayad, Z. A. Detection of Neovessels in Atherosclerotic Plaques of Rabbits Using Dynamic Contrast Enhanced MRI and 18F-FDG PET. Arterioscler. Thromb. Vasc. Biol. 2008, 28, 1311–1317.
27. Dong, L.; Kerwin, W. S.; Chen, H.; Chu, B.; Underhill, H. R.; Neradilek, M. B.; Hatsukami, T. S.; Yuan, C.; Zhao, X.-Q. Carotid Artery Atherosclerosis: Effect of Intensive Lipid Therapy on the Vasa Vasorum--Evaluation by Using Dynamic Contrast-Enhanced MR Imaging. Radiology 2011, 260, 224–231.
28. Kerwin, W.; Hooker, A.; Spilker, M.; Vicini, P.; Ferguson, M.; Hatsukami, T.; Yuan, C. Quantitative Magnetic Resonance Imaging Analysis of Neovasculature Volume in Carotid Atherosclerotic Plaque. Circulation 2003, 107, 851–856.
29. Moreno, P. R.; Purushothaman, K. R.; Fuster, V.; Echeverri, D.; Truszczynska, H.; Sharma, S. K.; Badimon, J. J.; O'Connor, W. N. Plaque Neovascularization Is Increased in Ruptured Atherosclerotic Lesions of Human Aorta: Implications for Plaque Vulnerability. Circulation 2004, 110, 2032–2038.

30. Kerwin, W. S.; O'Brien, K. D.; Ferguson, M. S.; Polissar, N.; Hatsukami, T. S.; Yuan, C. Inflammation in Carotid Atherosclerotic Plaque: A Dynamic Contrast-Enhanced MR Imaging Study. Radiology 2006, 241, 459–468.
31. Calcagno, C.; Vucic, E.; Mani, V.; Goldschlager, G.; Fayad, Z. A. Reproducibility of Black Blood Dynamic Contrast-Enhanced Magnetic Resonance Imaging in Aortic Plaques of Atherosclerotic Rabbits. J Magn Reson Imaging 2010, 32, 191–198.
32. Kershaw, L. E.; Cheng, H.-L. M. A General Dual-Bolus Approach for Quantitative DCE-MRI. Magn. Reson. Imaging 2011, 29, 160–166.
33. Haacke, E. M., Brown, R. W., Thompson, M. R., and Venkatesan, R. (1999). Magnetic Resonance Imaging, Physical Principles and Sequence Design. Wiley, New York.
34. Kerwin, W. S.; Cai, J.; Yuan, C. Noise and Motion Correction in Dynamic Contrast-Enhanced MRI for Analysis of Atherosclerotic Lesions. Magn. Reson. Med. 2002, 47, 1211–1217.
35. Parker, G. J. M.; Roberts, C.; Macdonald, A.; Buonaccorsi, G. A.; Cheung, S.; Buckley, D. L.; Jackson, A.; Watson, Y.; Davies, K.; Jayson, G. C. Experimentally-Derived Functional Form for a Population-Averaged High-Temporal-Resolution Arterial Input Function for Dynamic Contrast-Enhanced MRI. Magn. Reson. Med. 2006, 56, 993–1000.
36. Yankeelov, T. E.; Luci, J. J.; Lepage, M.; Li, R.; Debusk, L.; Lin, P. C.; Price, R. R.; Gore, J. C. Quantitative Pharmacokinetic Analysis of DCE-MRI Data without an Arterial Input Function: A Reference Region Model. Magn. Reson. Imaging 2005, 23, 519–529.

Acknowledgements

M.E.L. is supported by the International Atherosclerosis Society and by the Foundation "De Drie Lichten" in The Netherlands. This work was supported by the National Heart, Lung, and Blood Institute, National Institutes of Health, as a Program of Excellence in Nanotechnology (PEN) Award, Contract #HHSN268201000045C, as well as by R01 EB009638 (Z.A.F.) and R01 CA155432 (W.J.M.M.).